The *all-trans*-retinal dimer series of lipofuscin pigments in retinal pigment epithelial cells in a recessive Stargardt disease model

So R. Kim*, Young P. Jang*†, Steffen Jockusch‡, Nathan E. Fishkin‡, Nicholas J. Turro‡, and Janet R. Sparrow*§¶

Departments of *Ophthalmology, ‡Chemistry, and §Pathology and Cell Biology, Columbia University, New York, NY 10032

Edited by John E. Dowling, Harvard University, Cambridge, MA, and approved October 17, 2007 (received for review September 14, 2007)

The bis-retinoid pigments that accumulate in retinal pigment epithelial cells as lipofuscin are associated with inherited and age-related retinal disease. In addition to A2E and related *cis* isomers, we previously showed that condensation of two molecules of *all-trans*-retinal leads to the formation of a protonated Schiff base conjugate, *all-trans*-retinal dimer-phosphatidylethanolamine. Here we report the characterization of the related pigments, *all-trans*-retinal dimer-ethanolamine and unconjugated *all-trans*-retinal dimer, in human and mouse retinal pigment epithelium. In eyecups of *Abcr*$^{-/-}$ mice, a model of recessive Stargardt macular degeneration, *all-trans*-retinal dimer-phosphatidylethanolamine was increased relative to wild type and was more abundant than A2E. Total pigment of the *all-trans*-retinal dimer series (sum of *all-trans*-retinal dimer-phosphatidylethanolamine, *all-trans*-retinal dimer-ethanolamine, and *all-trans*-retinal dimer) increased with age in *Abcr*$^{-/-}$ mice and was modulated by amino acid variants in Rpe65. In *in vitro* assays, enzyme-mediated hydrolysis of *all-trans*-retinal dimer-phosphatidylethanolamine generated *all-trans*-retinal dimer-ethanolamine, and protonation/deprotonation of the Schiff base nitrogen of *all-trans*-retinal dimer-ethanolamine was pH-dependent. Unconjugated *all-trans*-retinal dimer was a more efficient generator of singlet oxygen than A2E, and the *all-trans*-retinal dimer series was more reactive with singlet oxygen than was A2E. By analyzing chromatographic properties and UV-visible spectra together with mass spectrometry, mono- and bis-oxygenated *all-trans*-retinal dimer photoproducts were detected in *Abcr*$^{-/-}$ mice. The latter findings are significant to an understanding of the adverse effects of retinal pigment epithelial cell lipofuscin.

macular degeneration | retinal pigment epithelium | bis-retinoid

The lipofuscin fluorophores that accumulate with age in retinal pigment epithelial (RPE) cells of the eye originate, for the most part, in photoreceptor cells and are deposited in the RPE when these cells phagocytose shed outer segment membrane (1). A number of observations over the years have also indicated that the deposition of lipofuscin fluorophores in RPE depends on vitamin A availability and on visual cycle function. For instance, RPE lipofuscin accumulation is reduced by dietary deficiency in vitamin A (1), by pharmacological agents that reduce serum vitamin A (2), and by genetic variants and small molecules that limit visual cycle kinetics (3, 4).

The first of the vitamin A aldehyde derivatives to be identified in RPE lipofuscin was the bisretinoid A2E (1, 5, 6), followed by a C13–C14 *Z*-isomer of A2E (isoA2E) (6) and other minor isomers (7). A2E and its *cis*-isomers absorb at ≈440 nm and form in photoreceptor outer segments by a multistep biosynthetic pathway involving reactions between phosphatidylethanolamine (PE) and *all-trans*-retinal (atRAL) and the formation of the precursors dihydro-A2PE (8) and A2PE (9). We recently also identified an RPE pigment with ≈510-nm absorbance (10, 11). This compound, atRAL dimer-PE (Fig. 1), is generated when two molecules of atRAL condense to form an aldehyde-bearing dimer (atRAL dimer) (Fig. 1) that subsequently forms a conjugate with PE via a protonated Schiff base linkage. Here we show that in *Abca4*/*Abcr*$^{-/-}$ (*Abcr*$^{-/-}$) mice, a model of juvenile-onset recessive Stargardt macular dystrophy (12), atRAL dimer-PE is accumulated in even greater abundance than A2E. We also demonstrate that phosphate cleavage of atRAL dimer-PE yields atRAL dimer-ethanolamine (atRAL dimer-E) (Fig. 1), an RPE lipofuscin fluorophore not previously identified in human and mouse RPE. In RPE isolated from human eyes and in the lipofuscin-filled RPE of *Abcr*$^{-/-}$ mice, we have identified not only atRAL dimer-PE, atRAL dimer-E, and unconjugated atRAL dimer (Fig. 1) but also mono- and bis-oxygenated photoproducts of atRAL dimer. This work provides further insight into the composition of RPE lipofuscin and a better understanding of properties of individual lipofuscin chromophores, information that is fundamental to our understanding of blinding retinal disorders associated with the accumulation of RPE lipofuscin.

Results

The Pigments atRAL Dimer-E, atRAL Dimer-PE, and Unconjugated atRAL Dimer Are Present in *Abcr*$^{-/-}$ Mouse Eyecups and in RPE of Human Eyes. Because *Abcr*-null mutant mice serve as a model of recessive Stargardt disease and have been shown to accumulate RPE lipofuscin fluorophores in abundance (3, 12), chloroform/methanol extracts of posterior eyecups of *Abcr*$^{-/-}$ mice were analyzed by reverse-phase HPLC. As expected, monitoring at 430 nm led to the detection of A2E (λ_{max} = 338 and 447 nm), isoA2E (λ_{max} = 337 and 426 nm), and other minor *cis*-isomers of A2E (6, 7) (Fig. 2*A*). Moreover, on the basis of UV-visible absorbance spectra and retention times (R_t) that corresponded to the authentic standards, peaks in the extract could also be assigned to atRAL dimer-E (R_t = 17.1 min; λ_{max} = 289 and 510 nm), atRAL dimer-PE (R_t = 27.3 min; λ_{max} = 290 and 511 nm), and unconjugated atRAL dimer (R_t = 34 min; λ_{max} = 290 and 432 nm). A representative overlay of C18 column chromatograms generated by injections of tissue extracts and authentic standards is shown in Fig. 2*A*. atRAL dimer-E, the ethanolamine Schiff base conjugate of atRAL dimer that has not previously been detected in tissue extracts, has a mass similar to A2E/isoA2E (A2E, 592; atRAL dimer-E, 594), and isoA2E and

Author contributions: S.R.K. and Y.P.J. contributed equally to this work; S.R.K., Y.P.J., S.J., and J.R.S. designed research; S.R.K., Y.P.J., S.J., and J.R.S. performed research; N.E.F., N.J.T., and J.R.S. contributed new reagents/analytic tools; S.R.K., Y.P.J., S.J., and J.R.S. analyzed data; and S.R.K., Y.P.J., S.J., and J.R.S. wrote the paper.

The authors declare no conflict of interest.

This article is a PNAS Direct Submission.

†Present address: College of Pharmacy, Kyung Hee University, Hoegi-dong, Dongdaemun-gu, Seoul 130-701, South Korea.

¶To whom correspondence should be addressed at: Department of Ophthalmology, Columbia University, 630 West 168th Street, New York, NY 10032. E-mail: jrs88@columbia.edu.

This article contains supporting information online at www.pnas.org/cgi/content/full/0708714104/DC1.

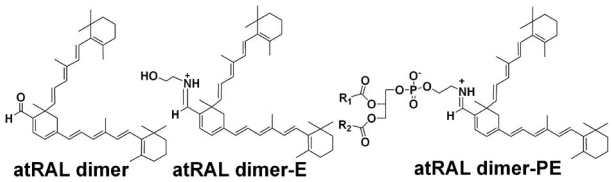

Fig. 1. Structures of the atRAL dimer series of RPE lipofuscin pigments, atRAL dimer, atRAL dimer-E, and atRAL dimer-PE.

atRAL dimer-E elute with similar retention times. However, in the expanded chromatogram generated with 510-nm monitoring and presented in Fig. 2*A Right*, the separation of isoA2E and atRAL dimer-E is clear. Given their respective absorbance maxima, detection of A2E, iso-A2E, and unconjugated atRAL dimer was favored with 430-nm monitoring whereas the protonated Schiff base compounds atRAL dimer-PE and atRAL dimer-E were favored at 510 nm. With chromatographic monitoring at 510 nm, atRAL dimer-PE exhibited a peak height that was considerably greater than A2E (Fig. 2*A Lower Right*).

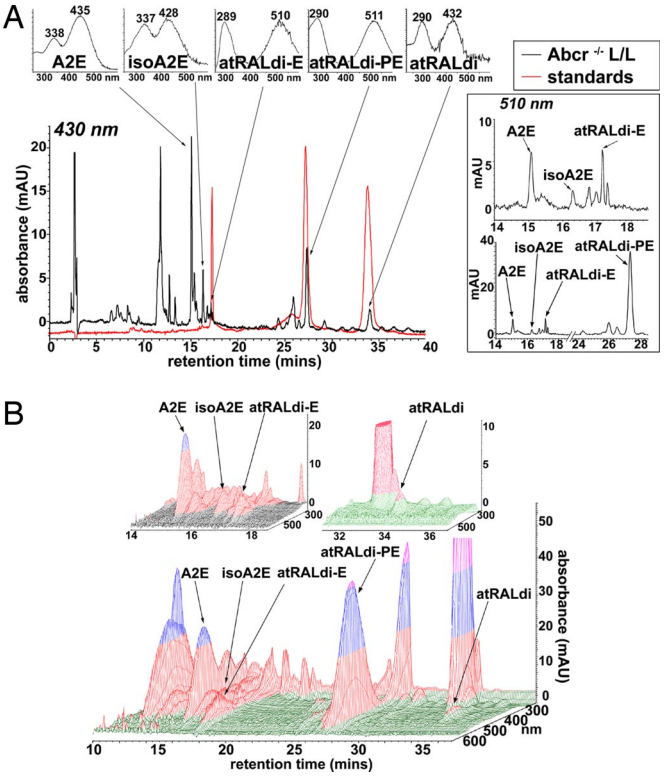

Fig. 2. Two- and three-dimensional display of HPLC chromatograms demonstrating the detection of atRAL-derived lipofuscin chromophores in extracts of eyecups from *Abcr*$^{-/-}$ mice. Mice were homozygous for Rpe65 Leu-450 (11 months old; pooled sample of eight eyecups). (*A Left Lower*) HPLC chromatograms obtained when injectant was eyecup extract (black) and a mixture of three standards (red): atRAL dimer-phosphatidylethanolamine, atRAL dimer-E, and unconjugated atRAL dimer. C18 column, 430-nm monitoring, and a gradient of acetonitrile and water (acetonitrile:water = 85:15 → 100:0 for 15 min; 0.8 ml/min) with 0.1% of TFA was used for mobile phase. (*A Left Upper*) UV-visible absorbance spectra corresponding to A2E, isoA2E, atRALdi-E, atRALdi-PE, and atRAL dimer (atRALdi). (*A Right*) Monitoring at 510 nm with chromatogram expanded between retention times of 14–18 min (*A Right Upper*) and monitoring at 510 nm with chromatogram expanded between 14 and 28 min (*A Right Lower*). (*B*) Three-dimensional display of retention time, wavelength (270–600 nm), and photodiode array absorbance data obtained by HPLC for the chromatogram in *A*.

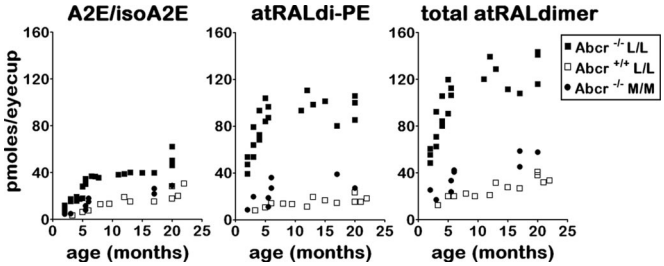

Fig. 3. HPLC quantitation of RPE lipofuscin pigments in eyecups of *Abcr*$^{-/-}$ and *Abcr*$^{+/+}$ mice and in *Abcr*$^{-/-}$ mice genotyped for Rpe65 Leu450Met. Levels of A2E and isoA2E (measured separately and summed, A2E/isoA2E), atRALdi-PE, and total atRAL dimer series (atRAL dimer-phosphatidylethanolamine, atRAL dimer-E, and atRAL dimer measured separately and summed) plotted as a function of age. Detection was at 430 nm (A2E, atRALdi) or 500 nm (atRAL di-PE, atRALdi-E). Mice were homozygous for Rpe65 Leu-450 (L/L) or Rpe65 Met-450 (M/M). Each data point is from a single sample, with two to six eyes per sample.

Three-dimensional analysis of the HPLC chromatograms (Fig. 2*B*) confirmed peak purity.

The bisretinoid pigments A2E, isoA2E, atRAL dimer-PE, atRAL dimer-E, and atRAL dimer were also present in extracts of human RPE/choroid. In supporting information (SI) Fig. 6 is shown a representative overlay of a C18 column chromatogram generated by injection of authentic standards, by injection of human RPE/choroid extract, or by coinjection of standard and extract. For each of these compounds peak authentication was corroborated by the increase in peak height observed when authentic standards were coinjected with RPE/choroid extract.

HPLC Quantitation of RPE Lipofuscin Pigments. Quantitation by integrating peak areas revealed that atRAL dimer-PE was considerably increased in *Abcr*$^{-/-}$ mice relative to *Abcr*$^{+/+}$ mice (Fig. 3). Importantly, in *Abcr*$^{-/-}$ mice levels of atRAL dimer-PE (monitoring at 510 nm) were also higher than the amounts of A2E (430-nm detection) across a range of ages (Fig. 3). Because atRAL dimer-PE, atRAL dimer-E, and unconjugated atRAL dimer are related compounds (see below), we also summed picomole levels obtained for atRAL dimer-PE, atRAL dimer-E, and unconjugated atRAL dimer (total atRAL dimer series) at various ages and observed an age-associated increase in these pigments (Fig. 3). Total pigment of the atRAL dimer series was also increased in *Abcr*$^{-/-}$ mice relative to wild type (Fig. 3). Additionally, in *Abcr*$^{-/-}$ mice homozygous for the Leu-450 allele of Rpe65, levels of atRAL dimer-PE and total atRAL dimer series were greater than in mice expressing methionine at position 450 (Fig. 3).

Interconversion of Compounds of the atRAL Dimer Series. Relationships within the atRAL dimer series of compounds were apparent from two lines of investigation. First, enzyme-mediated phosphate cleavage of atRAL dimer-PE generated atRAL dimer-E. Specifically, incubating DP-atRAL dimer-PE with phospholipase D (PLD) for 3 h at 37°C resulted in the appearance of a peak at ≈4.5 min that by UV/visible absorbance (λ_{max} = 510 and 286 nm) and coinjection with authentic standard could be identified as atRAL dimer-E (SI Fig. 7 *C* and *D*). At the same time, the peak attributable to DP-atRAL dimer-PE was diminished. This observation indicated that atRAL dimer-PE is the precursor of atRAL dimer-E and that the latter can be generated from the former by enzymatic hydrolysis. Interestingly, however, under conditions of our *in vitro* assay, PLD-mediated cleavage of atRAL dimer-PE was less efficient than PLD-mediated hydrolysis of A2PE (and release of A2E) (SI Fig. 7, compare *E* and *F*).

The atRAL dimer-conjugates, atRAL dimer-PE and atRAL

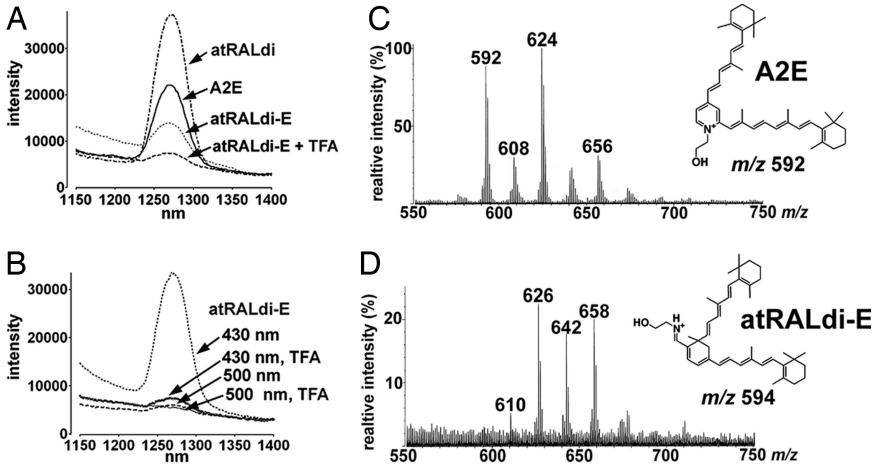

Fig. 4. Singlet oxygen generation and quenching. (*A* and *B*) Phosphorescence of singlet oxygen generated from A2E, atRALdi-E, and atRALdi. (*A*) A2E, atRALdi, and atRALdi-E (50 μM in CCl_4) were irradiated at 430 nm, and the generation of singlet oxygen was detected by its phosphorescence in the near infrared region. atRAL di-E was irradiated in the presence of TFA (atRALdi-E + TFA) or the absence of TFA (atRALdi-E) to test for the effect of protonation of the Schiff base nitrogen on the singlet oxygen yield. (*B*) Effect of protonation of atRALdi-E and illumination wavelength on the generation of singlet oxygen. atRALdi-E was excited at either 430 nm or 500 nm in the presence or absence of TFA. (*C* and *D*) Comparison of tendency of A2E and atRAL dimer-E (atRALdi-E) to quench singlet oxygen. A2E (*C*) and atRALdi-E (*D*) were oxidized by singlet oxygen generated from the endoperoxide of 1,4-dimethylnaphthalene. FAB-MS spectra are shown. A2E and atRALdi-E are detected as molecular ion peaks at *m/z* ratios of 592 and 594, respectively.

dimer-E, contain an imine function group (—C═N—) with a protonation state that is pH-dependent (10). Accordingly, by recording absorbance spectra of synthetic atRAL dimer-E solubilized in DPBS buffer solution as the pH of the buffer was changed from 3.3 to 4.1, we observed a hypsochromic shift in absorbance as the Schiff base was deprotonated (SI Fig. 8). The presence of both the 430-nm and 510-nm peaks at pH 3.85 was indicative of the presence of both the deprotonated and protonated forms of the Schiff base pigment.

Phosphorescence Detection of Singlet Oxygen. Because photoexcitation of A2E has been shown to generate singlet oxygen (13), we compared the phosphorescence spectrum of singlet oxygen generated with irradiation of A2E, unconjugated atRAL dimer, atRAL dimer-E, and atRAL dimer-E (H^+, protonated) at 430 nm. Luminescence studies based on the detection of a characteristic phosphorescence at 1,270 nm confirmed the generation of singlet oxygen upon photoexcitation of A2E. As shown in Fig. 4*A*, the intensity of the phosphorescence at 1,270 nm was more pronounced for unconjugated atRAL dimer than for A2E. Weaker luminescence was generated with protonated atRAL dimer-E.

Excitation at wavelengths in the blue region favors A2E and unconjugated atRAL dimer, whereas atRAL dimer-PE and atRAL dimer-E maximally absorb at ≈510 nm. Thus, we also compared the singlet oxygen phosphorescence spectrum generated when atRAL dimer-E was irradiated at 430 nm versus 500 nm and under acidic (to favor protonation) and nonacidic conditions (Fig. 4*B*). In these experiments using atRAL dimer-E, data also pertain to atRAL dimer-PE, because the phospholipid moiety does not make a contribution to the photoreactivity. With excitation at 500 nm, whether in the presence or absence of acid (trifluoroacetic acid, TFA), phosphorescence centered at 1,270 nm was negligible. On the other hand, the luminescence peak at 1,270 nm was pronounced with irradiation at 430 nm in the absence of TFA, conditions that promote deprotonation of atRAL dimer-E. Only weak phosphorescence was detectable with excitation at 430 nm and TFA, the latter acidic conditions supporting protonation. These findings indicate that, with deprotonation or with deprotonation/hydrolysis, photosensitization of the atRAL dimer compounds is increased.

To also compare atRAL dimer-E with A2E in terms of singlet oxygen reaction rates, we used the aromatic endoperoxide of 1,4-dimethylnaphthalene to generate singlet oxygen upon thermal decomposition (13). After mixtures of the endoperoxide of 1,4-dimethylnaphthalene with A2E and atRAL dimer-E were incubated, features of the collected fast atom bombardment ionization mass spectrometry (FAB-MS) spectra indicated that, as compared with A2E, atRAL dimer-E reacted more readily with singlet oxygen to become oxidized (Fig. 4). For instance, whereas a molecular ion peak corresponding to A2E (*m/z* 592) was detectable in the A2E/endoperoxide mixture (Fig. 4*C*), no *m/z* peak attributable to atRAL dimer-E (*m/z* 594) was detectable in the atRAL dimer-E/endoperoxide mixture (Fig. 4*D*). This observation indicated that, in the case of atRAL dimer-E, the entire starting compound had undergone oxidation. For both the atRAL dimer-E- and A2E-containing mixtures, a series of *m/z* +16 peaks (A2E: *m/z* 608, 624, 640, and 656; atRAL dimer-E: *m/z* 610, 626, 642, and 658) were present that reflected the addition of oxygens to the respective polyene structures (Fig. 4 *C* and *D*). However, in the case of the A2E/endoperoxide mixture the *m/z* 624 peak (Fig. 4*C*), indicative of monoperoxy-A2E, was most prominent (14), whereas with the atRAL dimer-E/endoperoxide mixture oxidized species bearing both one (*m/z* 626) and two (*m/z* 658) peroxides were prominent (Fig. 4*D*). The conclusion that the polyene side arms of atRAL dimer readily oxidize was corroborated by the finding that atRAL dimer also exhibited a greater tendency to undergo photooxidation than A2E (SI Fig. 9). In these experiments photooxidation was induced by irradiation at 430 nm and was monitored chromatographically as a consumption of the starting samples of atRAL dimer and A2E.

Oxidized atRAL Dimer in *Abcr*$^{-/-}$ Mouse Eyecups. Because unconjugated atRAL dimer can serve as a photosensitizer for the generation of singlet oxygen (Fig. 4), we next sought to detect oxidized forms of atRAL dimer in retinal tissues. To ascertain criteria for the identification of oxidized forms of atRAL dimer (oxo-atRAL dimer), we characterized the oxidation products generated by oxidizing agents that add one (*meta*-chloroperoxybenzoic acid, MCPBA), or two (endoperoxide of 1,4-dimethylnaphthalene) oxygen atoms at a time to A2E (14). For analysis, we used mass spectrometry, we monitored HPLC

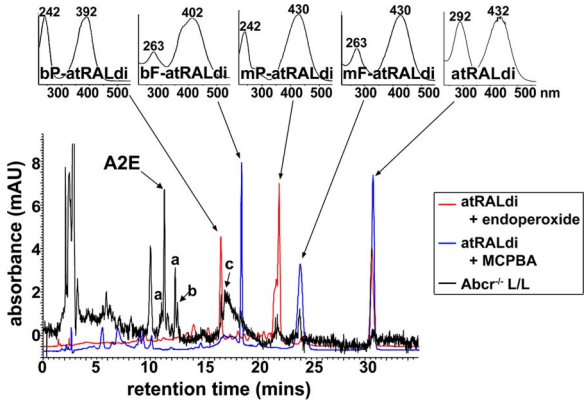

Fig. 5. Detection of photooxidized products of the RPE lipofuscin pigment atRAL dimer (atRALdi) in extracts of *Abcr*$^{-/-}$ mouse eyecups. (*Lower*) Chromatographic overlay of HPLC profiles generated with samples of atRALdi plus endoperoxide of 1,4-dimethylnaphthalene (red), atRALdi plus MCPBA (blue), or extract of *Abcr*$^{-/-}$ posterior eyecups (Rpe65 Leu-450; age, 12 months). (*Upper*) UV-visible absorbance of atRALdi and oxidized products of atRALdi. bP-atRALdi, bisperoxy-atRALdi; bF-atRALdi, bisfurano-atRALdi; mP-atRALdi, monoperoxy-atRALdi; mF-atRALdi, monofurano-atRALdi. a, *cis*-isomers of A2E; b, atRAL dimer-E; c, atRAL dimer-PE.

retention times, and we used UV-visible spectroscopy to detect hypsochromic absorbance shifts reflecting oxidation-associated loss of double bond conjugation (14) (as detailed in *SI Text*). Accordingly, we identified four oxo-atRAL dimer species, mono- and bis-peroxy-atRAL dimer generated by addition of molecular singlet oxygen, and mono- and bis-furano-atRAL dimer generated by reaction of atRAL dimer with MCPBA, the source of an electrophilic oxygen (SI Fig. 10).

We subsequently sought to identify these oxidized forms of atRAL dimer in extracts of posterior eyecups harvested from *Abcr*$^{-/-}$ mice. Our approach was to overlay C18 column chromatograms generated by HPLC injection of the *Abcr*$^{-/-}$ mouse extract with chromatograms produced from oxo-atRAL dimer samples (generated by incubating atRAL dimer with MCPBA or endoperoxide of 1,4-dimethylnaphthalene as described above) and to observe for peaks eluting earlier than atRAL dimer. The earlier elution is to be expected of oxidized products having increased polarity. Accordingly, four peaks in the *Abcr*$^{-/-}$ eyecup extract eluted before atRAL dimer and overlapped with peaks in the MCPBA/atRAL dimer or endoperoxide/atRAL dimer incubation mixtures (Fig. 5). On the basis of retention time and UV-visible absorbance, these compounds were identified as (in order of elution) bisperoxy-atRAL dimer (λ_{max} = 242 and 392 nm; R_t = 16.6 min), bisfuran-atRAL dimer (λ_{max} = 263 and 402 nm; R_t = 18.2 min), monoperoxy-atRAL dimer (λ_{max} = 242 and 432 nm; R_t = 21.9 min), and monofurano-atRAL dimer (λ_{max} = 263 and 430 nm; R_t = 23.9 min).

Discussion

Clinical and laboratory evidence increasingly implicates anomalous lipofuscin accumulation in the pathogenesis of RPE cell degeneration in patients with recessive Stargardt disease, atrophic age-related macular degeneration, and other forms of macular disease (2, 15, 16). Our interest in the atRAL dimer series of RPE lipofuscin pigments originated with the detection of unconjugated atRAL dimer in isolated bovine photoreceptor outer segments that were incubated with exogenous atRAL or irradiated to induce photoisomerization and release of endogenous atRAL (10). We demonstrated that the synthetic compound generated by base-catalyzed condensation of two atRAL had the same UV/visible absorbance (λ_{max} = 295 and 432 nm) and HPLC retention time as the compound in the incubated outer segments. By mass spectrometry we determined that atRAL dimer had a mass of 550 (10). In addition, by ^{1}H-NMR, together with quantum chemical calculations and circular dichroism, the structure and lowest-energy conformations of atRAL dimer were studied (11). Anticipating that atRAL dimer could form a Schiff base conjugate with amino moieties via its aldehyde group, we also reacted atRAL dimer with ethanolamine and confirmed the structure of the product (atRAL dimer-E) by ^{1}H-NMR (10). In conjunction with this we showed that reaction of atRAL dimer with PE, a phospholipid that is abundant in outer segments, produced a compound with a UV/visible absorbance that was dramatically red-shifted; this pigment was detected in eyecups of *Abcr*$^{-/-}$ mice (10). In the current study we now show that unconjugated atRAL dimer and atRAL dimer-E, a molecule similar in structure to atRAL dimer-PE but without the phosphatidyl group, are also extractable from *Abcr*$^{-/-}$ mouse eyecups and from human RPE. The pigments we have identified as atRAL dimer, atRAL dimer-E, and atRAL dimer-PE in the tissue samples studied in the present work all have the same UV/visible absorbances and retention times as the synthetic compounds used for the earlier structural characterizations.

Besides their origin from reactions of atRAL, we demonstrate that atRAL dimer conjugates exhibit other features similar to the previously characterized RPE lipofuscin pigment A2E. For instance, these pigments are elevated in *Abcr*$^{-/-}$ mice just as is A2E; indeed, atRAL dimer-PE alone is more abundant than is A2E. Levels of A2E (3) and of the atRAL dimer-series (current study) also vary with the murine Rpe65 Leu450Met polymorphism, an amino acid substitution that alters the kinetics of the retinoid cycle (17–19). For all of these lipofuscin chromophores, the polyene structures of the atRAL-derived side arms, together with double bonds within the six-membered rings, provide the extended conjugation systems that confer absorbance maxima in the visible range of the spectrum. In the case of atRAL dimer-PE and atRAL dimer-E, a further red shift occurs with protonation of the Schiff base nitrogen.

Nevertheless, although A2E/isoA2E, atRALdi-E, and atRAL dimer-phosphatidylethanolamine (atRALdi-PE) are all bisretinoid compounds, there are important differences among them. For instance, A2E and isoA2E are pyridinium salts containing a quaternary amine nitrogen that cannot be deprotonated or reprotonated (6, 20). The compounds atRAL dimer-E and atRAL dimer-PE are, on the other hand, dimers of atRAL attached to PE via a Schiff base linkage that is protonated under the conditions in which it is isolated (10). By recording changes in absorbance of atRAL dimer-E, we found that the protonation state of the imine nitrogen is pH-dependent with an apparent imine pK_a of 3.8 under our conditions. *N*-retinylidene Schiff bases typically have a pK_a from 6 to 7 (21, 22); however, strong electron-withdrawing groups proximal to the Schiff base nitrogen are known to destabilize the N—H bond (23). It is reasonable, then, that the electron-withdrawing oxygen in atRAL dimer-E has a significant effect on lowering the apparent pK_a. atRAL dimer-PE, by contrast, may be expected to have a higher pK_a due to the negatively charged phosphate that can stabilize the nearby N—H bond. A hydrophobic milieu can also increase the pK_a of *N*-retinylidene Schiff bases (24). So it is possible that atRAL dimer-PE, when housed in lysosomes (pH $\approx$ 5) with a more hydrophobic milieu, could exist largely in the protonated Schiff base form. Overall, the detection of both protonated atRAL dimer conjugates (atRAL dimer-PE and atRAL dimer-E) and unprotonated unconjugated atRAL dimer in extracts of RPE lipofuscin suggests conditions permitting both protonated and unprotonated forms.

We present evidence that atRAL dimer-PE can serve as a precursor for atRAL dimer-E, with an enzymatic hydrolytic activity serving to remove the phosphatidyl group from atRAL

dimer-PE, thereby generating atRAL dimer-E. Just as the precursor A2PE is cleaved within RPE cell lysosomes to generate A2E, we postulate that the conversion of atRAL dimer-PE to atRAL dimer-E could occur in the lysosomal compartment of the RPE. The possibility remains, however, that atRAL dimer-E could also form by direct Schiff base conjugation of atRAL dimer with ethanolamine. Schiff base hydrolysis of atRAL dimer-PE and atRAL dimer-E can also yield atRAL dimer, and it is likely that the balance amongst these pigments can be shifted by pH and the extent of hydrophobicity of the cellular environment. Another pigment in $Abcr^{-/-}$ mouse eyecups with absorbance maxima at ≈285 and 510 nm, has been reported to be dihydro-A2PE (A2PE-H_2) (25), a precursor of A2E (6); however, identification was not confirmed with a synthetic standard. We recently demonstrated that dihydro-A2PE has UV-visible absorbance maxima at 490 and 330 nm in acetonitrile (8).

An understanding of the adverse effects of the photooxidation of RPE lipofuscin pigments has been advanced by studies of A2E. It is now well known that short-wavelength visible-light irradiation of A2E leads to the formation of singlet oxygen and other reactive forms of oxygen that subsequently add to carbon–carbon double bonds along the side arms of the molecule (13, 26). The reactive moieties generated by A2E photooxidation and cleavage, including endoperoxides and aldehydes (14), likely account for the adverse effects observed when RPE cells that have accumulated A2E are irradiated at 430 nm (27–30). In the present work we found that unconjugated atRAL dimer is a more efficient generator of singlet oxygen than A2E when irradiated at 430 nm. Significantly, our experiments with atRAL dimer-E also indicate that the atRAL dimer series of compounds react more efficiently with singlet oxygen. The electron density differences between A2E and atRAL dimer-E likely explain the greater susceptibility to oxidation exhibited by atRAL dimer-E. For instance, the short arm of the atRAL dimer moiety is likely to be more susceptible to oxidation because with only four double bond conjugations electron delocalization is reduced, and the resulting increased density of electrons makes the sp^2 carbons more vulnerable to attack. The long arm of atRAL dimer-E is also expected to be more electron-dense than the long arm of A2E because the pyridinium ring of A2E attracts electrons more strongly than does the cyclohexadiene ring of atRAL dimer. As is the case for A2E (14), the photooxidation of atRAL dimer would lead to a complex mixture of oxygen-containing moieties, and we have shown here that at least some of these include monooxygen- and dioxygen-containing heterocyclic rings that, by analogy with A2E oxidation, we have identified as furanoid oxides and cyclic peroxides, respectively. It is significant that these oxo-atRAL dimer compounds are present in hydrophobic extracts of eyecups isolated from $Abcr^{-/-}$ mice. Still other photooxidation products of atRAL dimer could include those with an aromatized core (10).

We propose that there are at least two biosynthetic pathways by which atRAL can form RPE lipofuscin pigments, one leading to the generation of A2E and its isomers (6) and the other leading to the production of the atRAL dimer series of compounds (10). Increased accumulation of RPE lipofuscin bisretinoid pigments is considered to be the cause of RPE atrophy in Stargardt disease, a macular degeneration with onset in the second decade of life. It is thus noteworthy that we report here that the atRAL dimer series of compounds constitutes the most abundant of the lipofuscin chromophores characterized thus far in $Abcr^{-/-}$ mice. The susceptibility to photooxidation exhibited by the unconjugated member of this group is likely to be significant to an understanding of the damaging effects of these compounds.

Experimental Procedures

Synthesis of Compounds. A2E (6), A2PE (9), atRAL dimer, atRAL dimer-E, and atRAL dimer-PE (Fig. 1) (10) were synthesized as previously described. The structures of synthesized standards of A2E/isoA2E and A2PE have been corroborated (5, 6, 9). The structure of a synthesized standard of atRAL dimer was confirmed by mass spectrometry, ^{1}H-NMR, and circular dichroism (10, 11), and the structure of atRAL dimer-E was corroborated by mass spectrometry and ^{1}H-NMR (10). All of the above compounds were purified by HPLC. Because synthesized A2PE and atRAL dimer-PE were produced by using dipalmitoyl-phosphatidylethanolamine (DP-PE), synthesized standards are DP-A2PE and DP-atRAL dimer-PE, respectively.

Tissue Extraction and HPLC Analysis. *Abca4*/*Abcr*-null mutant mice (albino) homozygous for *Rpe65-Leu-450* were generated, genotyped, and housed as previously reported (3). Posterior eyecups of mice and RPE/choroids harvested from human donor eyes (National Disease Research Interchange, Philadelphia) were homogenized in PBS by using a glass tissue grinder and extracted in chloroform/methanol (2:1). Extracts were subsequently filtered through cotton and passed through a reverse-phase cartridge (C8 Sep-Pak; Millipore) with 0.1% TFA (Aldrich) in methanol. After evaporation of solvent under argon gas, the extract was dissolved in 50% methanolic chloroform containing 0.1% TFA. An Alliance system (Waters) equipped with 2695 Separation Module, 2996 Photodiode Array Detector, and a 2475 Multi λ Fluorescence Detector and operating with Empower software was used for HPLC analysis. An Atlantis dC18 column (3 μm, 4.6 × 150 mm; Waters) and a Delta Pak C4 column (5 μm, 3.9 × 150 mm; Waters) were used. Gradients of water and acetonitrile (Fisher) with 0.1% of TFA were used for mobile phase; details are provided in the figure legends. HPLC quantification was carried out by using Empower software to determine peak areas. Molar quantity per murine eye was determined by using calibration curves constructed from known concentrations of purified external standards and by normalizing to the ratio of the HPLC injection volume (10 μl) versus total extract volume.

PLD-Mediated Cleavage. Phosphate cleavage of A2PE and atRAL dimer-PE in the presence of PLD (Sigma–Aldrich) was analyzed by *in vitro* assay as described in *SI Text*.

pH-Dependent Interconversion of atRAL Dimer-E and atRAL Dimer. Protonation/deprotonation of atRAL dimer-E was monitored by recording UV-visible spectra with change in pH as described in *SI Text*.

Phosphorescence Spectroscopy. The generation of singlet oxygen by irradiated (430 nm and 500 nm) A2E and atRAL dimer-E was measured by near infrared phosphorescence using a modified Fluorolog 2 (Horiba) equipped with a cooled Hamamatzu photomultiplier tube (NIR-PMT; H9170-45). As excitation source, a 450-W Xe-lamp (Osram) in conjunction with a double-grating monochromator was used. To minimize local photodecomposition due to the excitation of light, the solution was mixed with a magnetic stirrer during the measurement. All singlet oxygen phosphorescence experiments were performed in CCl_4 in the absence/presence of 0.1% TFA (pH ≈ 2.0).

Oxidation Conditions. A2E and atRAL dimer were oxidized by 430-nm irradiation and by incubation with endoperoxide of 1,4-dimethylnaphthalene (13) and MCPBA (Aldrich) as published (14) and as described in *SI Text*.

This work was supported by National Institutes of Health Grant EY 12951, the Steinbach Fund, the Foundation Fighting Blindness (J.R.S.), National Science Foundation Grant CHE-04-15516 (to N.J.T. and S.J.), and a grant from Research to Prevent Blindness to the Department of Ophthalmology.

1. Eldred GE (1998) in *The Retinal Pigment Epithelium*: *Function and Disease*, eds Marmor MF, Wolfensberger TJ (Oxford Univ Press, New York), pp 651–668.
2. Radu RA, Han Y, Bui TV, Nusinowitz S, Bok D, Lichter J, Widder K, Travis GH, Mata NL (2005) *Invest Ophthalmol Vis Sci* 46:4393–4401.
3. Kim SR, Fishkin N, Kong J, Nakanishi K, Allikmets R, Sparrow JR (2004) *Proc Natl Acad Sci USA* 101:11668–11672.
4. Maiti P, Kong J, Kim SR, Sparrow JR, Allikmets R, Rando RR (2006) *Biochemistry* 45:852–860.
5. Sakai N, Decatur J, Nakanishi K, Eldred GE (1996) *J Am Chem Soc* 118:1559–1560.
6. Parish CA, Hashimoto M, Nakanishi K, Dillon J, Sparrow JR (1998) *Proc Natl Acad Sci USA* 95:14609–14613.
7. Ben-Shabat S, Parish CA, Vollmer HR, Itagaki Y, Fishkin N, Nakanishi K, Sparrow JR (2002) *J Biol Chem* 277:7183–7190.
8. Kim SR, He J, Yanase E, Jang YP, Berova N, Sparrow JR, Nakanishi K (2007) *Biochemistry* 46:10122–10129.
9. Liu J, Itagaki Y, Ben-Shabat S, Nakanishi K, Sparrow JR (2000) *J Biol Chem* 275:29354–29360.
10. Fishkin N, Sparrow JR, Allikmets R, Nakanishi K (2005) *Proc Natl Acad Sci USA* 102:7091–7096.
11. Fishkin N, Pescitelli G, Sparrow JR, Nakanishi K, Berova N (2004) *Chirality* 16:637–641.
12. Weng J, Mata NL, Azarian SM, Tzekov RT, Birch DG, Travis GH (1999) *Cell* 98:13–23.
13. Ben-Shabat S, Itagaki Y, Jockusch S, Sparrow JR, Turro NJ, Nakanishi K (2002) *Angew Chem Int Ed* 41:814–817.
14. Jang YP, Matsuda H, Itagaki Y, Nakanishi K, Sparrow JR (2005) *J Biol Chem* 280:39732–39739.
15. Delori FC, Goger DG, Dorey CK (2001) *Invest Ophthalmol Vis Sci* 42:1855–1866.
16. Holz FG, Bellman C, Staudt S, Schutt F, Volcker HE (2001) *Invest Ophthalmol Vis Sci* 42:1051–1056.
17. Wenzel A, Reme CE, Williams TP, Hafezi F, Grimm C (2001) *J Neurosci* 21:53–58.
18. Nusinowitz S, Nguyen L, Radu RA, Kashani Z, Farber DB, Danciger M (2003) *Exp Eye Res* 77:627–638.
19. Lyubarsky AL, Savchenko AB, Morocco SB, Daniele LL, Redmond TM, Pugh EN (2005) *Biochemistry* 44:9880–9888.
20. Sparrow JR, Parish CA, Hashimoto M, Nakanishi K (1999) *Invest Ophthalmol Vis Sci* 40:2988–2995.
21. Blatz PE, Johnson RH, Mohler JH, al-Dilaimi SK, Dewhurst S, Erickson JO (1971) *Photochem Photobiol* 13:237–245.
22. Schaffer AM, Yamaoka T, Becker RS (1975) *Photochem Photobiol* 21:297–301.
23. Sheves M, Albeck A, Friedman N, Ottolenghi M (1986) *Proc Natl Acad Sci USA* 83:3262–3266.
24. Viguera AR, Villa MJ, Goni FM (1990) *J Biol Chem* 265:2527–2532.
25. Mata NL, Weng J, Travis GH (2000) *Proc Natl Acad Sci USA* 97:7154–7159.
26. Sparrow JR, Zhou J, Ben-Shabat S, Vollmer H, Itagaki Y, Nakanishi K (2002) *Invest Ophthalmol Vis Sci* 43:1222–1227.
27. Sparrow JR, Zhou J, Cai B (2003) *Invest Ophthalmol Vis Sci* 44:2245–2251.
28. Sparrow JR, Vollmer-Snarr HR, Zhou J, Jang YP, Jockusch S, Itagaki Y, Nakanishi K (2003) *J Biol Chem* 278:18207–18213.
29. Zhou J, Cai B, Jang YP, Pachydaki S, Schmidt AM, Sparrow JR (2005) *Exp Eye Res* 80:567–580.
30. Zhou J, Jang YP, Kim SR, Sparrow JR (2006) *Proc Natl Acad Sci USA* 103:16182–16187.